Inorg. Chem. **2005**, *44*, 3810–3817

Effects of Countercations on the Structures and Redox and Spectroscopic Properties of Diruthenium Catecholate Complexes with Ligand-Unsupported Ru–Ru Bonds

Ho-Chol Chang,[†,‡] Katsunori Mochizuki,[†] and Susumu Kitagawa*[,†]

Department of Synthetic Chemistry and Biological Chemistry, Graduate School of Engineering, Kyoto University, Katsura, Nishikyo-ku, Kyoto 615-8510, and PRESTO, Japan Science and Technology Agency, 4-1-8 Honcho, Kawaguchi, Saitama 332-0012, Japan

Received December 13, 2004

The molecular structures and physicochemical properties of diruthenium complexes with ligand-unsupported Ru–Ru bonds, generally formulated as $[A_2\{Ru_2(DTBCat)_4\}]$ (DTB = 3,5- or 3,6-di-*tert*-butyl; Cat^{2-} = catecholate), were studied in detail by changing the countercations. First, the binding structures of the cations in a family of $[\{A(DME)_n\}_2\{Ru_2(3,5\text{-}DTBCat)_4\}]$ ($n = 2$ for $A^+ = Li^+$ and Na^+ and $n = 1$ for $A^+ = K^+$ and Rb^+) were systematically examined to reveal the effects of the cations on the molecular structures and electrochemical properties. Second, the complex $(n\text{-}Bu_4N)_2[Ru_2(3,6\text{-}DTBCat)_4]$ with a cation-free structure was synthesized using tetra-*n*-butylammonium cations. The complex clearly demonstrates first that the ligand-unsupported Ru–Ru bonds are essentially stabilized by the dianionic nature of the catecholate derivatives without any other bridging or supporting species. In contrast, the redox potentials and absorption spectra of the complexes can sensitively respond to the countercations depending upon the polarity of the solvents.

1. Introduction

As is documented in numerous published reports, considerable attention has been paid to the development of dimetallic complexes with metal−metal bonds.[1] These studies have revealed that the molecular structures and physical properties of metal−metal-bonded compounds are affected by oxidation states,[2] substituents on the ligands,[3] and counterions.[4] Particularly, the synthetic, structural, and physicochemical studies of dimetallic structures containing *counteranions* are well-investigated,[5] because most of the counteranions have coordination ability to the axial position of the metal−metal bond, and easily construct polymeric structures. The continuing study provides a diversity of complexes, and has led to attractive properties depending on the counteranion.[6] On the other hand, the effects of cations on structures and physical properties in the solid state and solution have been less well-described for dimetallic com-

* Author to whom correspondence should be addressed. E-mail: kitagawa@sbchem.kyoto-u.ac.jp. Phone: +81-75-383-2733. Fax: +81-75-383-2732.

† Kyoto University.

‡ Japan Science and Technology Agency.

(1) (a) Cotton, F. A.; Walton, R. A. *Multiple Bonds Between Metal Atoms*, 2nd ed.; Oxford University Press: Oxford, England, 1993. (b) Boyar, E. B.; Robinson, S. D. *Coord. Chem. Rev.* **1983**, *50*, 109. (c) Cotton, F. A.; Eglin, J. L. *Inorg. Chim. Acta* **1992**, *198*−*200*, 13. (d) Aquino, M. A. S. *Coord. Chem. Rev.* **1998**, *170*, 141. (e) Cotton, F. A.; Lin, C.; Murillo, C. A. *Acc. Chem. Res.* **2001**, *34*, 759. (f) Collman, J. P.; Boulatov, R. *Angew. Chem., Int. Ed.* **2002**, *41*, 3948.

(2) (a) Cotton, F. A.; Yokochi, A. *Inorg. Chem.* **1997**, *36*, 567. (b) Prater, M. E.; Pence, L. E.; Clérac, R.; Finniss, G. M.; Campana, C.; Auban-Senzier, P.; Jérome, D.; Canadell, E.; Dunbar, K. R. *J. Am. Chem. Soc.* **1999**, *121*, 8005. (c) Hesschenbrouck, J.; Solari, E.; Scopelliti, R.; Floriani, C.; Re, N. *J. Organomet. Chem.* **2000**, *596*, 77. (d) Mitsumi, M.; Murase, T.; Kishida, H.; Yoshinari, T.; Ozawa, Y.; Toriumi, K.; Sonoyama, T.; Kitagawa, H.; Mitani, T. *J. Am. Chem. Soc.* **2001**, *123*; 11179−11192.

(3) (a) Ren, T. *Coord. Chem. Rev.* **1998**, *175*, 43. (b) Lin, C.; Ren, T.; Valente, E. J.; Zubkowski, J. D. *J. Chem. Soc., Dalton Trans.* **1998**, 571. (c) Kadish, K. M.; Wang, L.-L.; Thuriere, A.; Caemelbecke, E. V.; Bear, J. L. *Inorg. Chem.* **2003**, *42*, 834. (d) Mitsumi, M.; Umebayashi, S.; Ozawa, S.; Tadokoro, M.; Kawamura, H.; Toriumi, K. *Chem. Lett.* **2004**, 33, 970.

(4) (a) Krogmann, K. *Angew. Chem., Int. Ed. Engl.* **1969**, *8*, 35. (b) Lecrone, F. N.; Minot, M. J.; Perlstein, J. H. *Inorg. Nucl. Chem. Lett.* **1972**, *8*, 173. (c) Cotton, F. A.; Daniels, L. M.; Murillo, C. A.; Pascual, I. *Inorg. Chem. Commun.* **1998**, *1*. 1.

(5) (a) Collins, D. M.; Cotton, F. A.; Gage, L. D. *Inorg. Chem.* **1979**, *18*, 1712. (b) Bino, A.; Cotton, F. A.; Felthouse, T. R. *Inorg. Chem.* **1979**, *18*, 2599. (c) Bino, A.; Cotton, F. A. *Inorg. Chem.* **1979**, *18*, 3562. (c) Chakravarty, A. R.; Cotton, F. A.; Tocher, D. A. *Inorg. Chem.* **1985**, *24*, 1334. (d) Baranovskii, I. B.; Golubnichaya, M. A.; Dikareva, L. M.; Rotov, A. V.; Shchelokov, R. N.; Porai-Koshits, M. A. *Russ. J. Inorg. Chem.* **1986**, *31*, 1652.

(6) (a) Handa, M.; Sayama, Y.; Mikuriya, M.; Nukada, R.; Hiromitsu, I.; Kasuga, K. *Chem. Lett.* **1996**, 201. (b) William, Y. L.; Shum, W.; Miller, J. S. *J. Am. Chem. Soc.* **2002**, *124*, 9336.

10.1021/ic048250u CCC: $30.25
Published on Web 04/28/2005

Scheme 1. Synthetic Scheme for Diruthenium Complexes with Ligand-Unsupported Ru−Ru Bonds

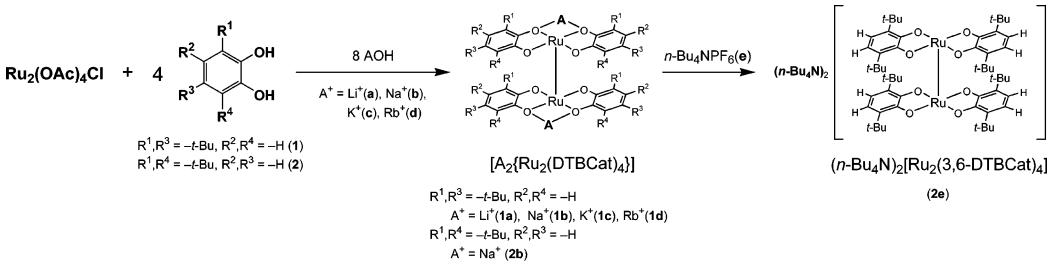

plexes accompanying by *countercations* represented by $[M_2X_8]^{n-}$ (X = halogen atom),[7] $[M_2(CO_3)_4]^{n-}$,[8] $[M_2(SO_4)_4]^{n-}$,[9] and $[M_2(HPO_4)_4]^{n-}$.[10]

In the preceding paper of this series,[11] we reported the synthesis and the structural and physicochemical diversity of a variety of diruthenium complexes, generally formulated as $[Na_n\{Ru_2(R_4Cat)_4\}]$ (n = 2 or 3; R_4 = F_4, Cl_4,[12] Br_4, H_4, 3,5-di-*t*-Bu, and 3,6-di-*t*-Bu), and clearly demonstrated that the complexes with ligand-unsupported Ru−Ru bonds can sensitively respond to redox reactions and ligand substituents on the basis of the greater degree of freedom in their molecular structures. Although special attention had not been paid to the interaction between the $[Ru_2(R_4Cat)_4]^{2-/3-}$ units and countercations in the literature, the countercations, Na^+, bind to the O_{Cat} atoms of R_4Cat^{2-} in all of the complexes. This situation calls into doubt the inherent stability of the ligand-unsupported Ru−Ru bonds. Therefore, in this paper, we describe the effects of the cation both in the solid state and in solution with various alkali-metal cations, Li^+, Na^+, K^+, and Rb^+. Furthermore, the challenging synthesis of a complex with a cation-free structure was carried out to minimize the effects of cations, and its structural and electrochemical properties were compared with those of the cation-bound complexes. We describe the effect of countercations on the molecular structures and physical properties of dinuclear complexes to give a new route for developing the usefulness of the M−M-bonded system as a molecular building block.

2. Experimental Section

2.1. Materials and Methods. Tetraacetatodiruthenium chloride ($Ru_2(OAc)_4Cl$),[13] [{$Na(DME)_2$}$_2${Ru_2(3,5-DTBCat)$_4$}] (**1b**),[11] and [Na_2{Ru_2(3,6-DTBCat)$_4$}] (**2b**)[11] were synthesized by literature methods. The other chemicals were purchased from Aldrich Chemical Co. (1,4,7,10,13,16-hexaoxacyclooctadecane (18-crown-6)), Tokyo Chemical Industry Co., Ltd. (3,5-di-*tert*-butylcatechol (3,5-DTBCatH_2) and tetra-*n*-butylammonium hexafluorophosphate (n-Bu_4NPF_6)), Wako Pure Chemical Industries, Ltd. (lithium hydroxide monohydrate ($LiOH\cdot H_2O$), Nacalai Tesque, Inc. (sodium hydroxide (NaOH) and potassium hydroxide (KOH)), and Kanto Kagaku (rubidium hydroxide (RbOH)). All of the solvents (tetrahydrofuran (THF), *n*-hexane (hexane), 1,2-dimethoxyethane (DME), and *N*,*N*-dimethylformamide (DMF)) were distilled by standard methods under a dinitrogen atmosphere. All synthetic operations were performed under a dinitrogen atmosphere.

2.2. Abbreviations for the Complexes. Each alphabet character followed by a number is assigned on the basis of the type of countercations included in each complex, Li^+ (**a**), Na^+ (**b**), K^+ (**c**), Rb^+ (**d**), and n-Bu_4N^+ (**e**) (Scheme 1). Because the single crystals and the polycrystalline samples of **2b** and **2e** have different compositions, these are distinguished by adding "s" in a subscript form after each abbreviation number for single crystalline samples.

2.3. Procedure for Preparation. For **1a**, **1c**, and **1d**, the following synthetic procedure was used. A THF suspension containing $Ru_2(OAc)_4Cl$, 4 equiv of 3,5-DTBCatH_2, and 8 equiv of AOH (A^+ = Li^+ (**1a**), K^+ (**1c**), and Rb^+ (**1d**)) were stirred for a day at room temperature. The red-purple suspensions were dried under vacuum, and then extracted with THF. The crystalline products were obtained by slow diffusion of DME onto the solutions.

[{Li(DME)$_2$}$_2${Ru$_2$(3,5-DTBCat)$_4$}] (1a). $Ru_2(OAc)_4Cl$ (237 mg, 0.50 mmol), 3,5-DTBCatH_2 (445 mg, 2.00 mmol), and $LiOH\cdot H_2O$ (168 mg, 4.00 mmol) were combined in THF to afford the red-purple crystals of **1a**. Yield: 175 mg (24%). Anal. Calcd for $C_{72}H_{120}Li_2O_{16}Ru_2$ (**1a**): C, 59.32; H, 8.30. Found: C, 59.10; H, 7.85. UV−vis−NIR (λ_{max}/nm (ϵ/$M^{-1}\cdot cm^{-1}$) in THF): 294 (27800), 501 (16500), 700 (sh).

[{K(DME)}$_2${Ru$_2$(3,5-DTBCat)$_4$}] (1c). $Ru_2(OAc)_4Cl$ (119 mg, 0.25 mmol), 3,5-DTBCatH_2 (222 mg, 1.00 mmol), and KOH (112 mg, 2.00 mmol) were combined in THF to afford the red-purple crystals of **1c**. Yield: 171 mg (51%). Anal. Calcd for $C_{64}H_{100}K_2O_{12}Ru_2$ (**1c**): C, 57.29; H, 7.51. Found: C, 56.75; H, 7.27. UV−vis−NIR (λ_{max}/nm (ϵ/$M^{-1}\cdot cm^{-1}$) in THF): 298 (24600), 494 (16800), 720 (sh).

[{Rb(DME)}$_2${Ru$_2$(3,5-DTBCat)$_4$}] (1d). $Ru_2(OAc)_4Cl$ (119 mg, 0.25 mmol), 3,5-DTBCatH_2 (222 mg, 1.00 mmol), and RbOH (205 mg, 2.00 mmol) were combined in THF to afford the red-purple crystals of **1d**. Yield: 172 mg (48%). Anal. Calcd for $C_{64}H_{100}O_{12}Rb_2Ru_2$ (**1d**): C, 53.58; H, 7.03. Found: C, 53.27; H, 6.96. UV−vis−NIR (λ_{max}/nm (ϵ/$M^{-1}\cdot cm^{-1}$) in THF): 299 (26400), 486 (17700), 570 (sh), 720 (sh).

(n-Bu$_4$N)$_2$[Ru$_2$(3,6-DTBCat)$_4$] (2e). A THF solution of **2b** (226 mg, 0.20 mmol) was combined with a THF solution containing n-Bu_4NPF_6 (155 mg, 0.40 mmol) with stirring at room temperature.

(7) (a) Cotton, F. A.; Harris, C. B. *Inorg. Chem.* **1965**, *4*, 330. (b) Brencic, J. V.; Cotton, F. A. *Inorg. Chem.* **1969**, *8*, 7. (c) Cotton, F. A.; DeBoer, B. G.; Jeremic, M. *Inorg. Chem.* **1970**, *9*, 2143. (d) Cotton, F. A.; Hall, W. T. *Inorg. Chem.* **1977**, *16*, 1867. (e) Cotton, F. A.; Mott, G. N. *J. Am. Chem. Soc.* **1982**, *104*, 6781.
(8) (a) Lindsay, A. J.; Wilkinson, G.; Motevalli, M.; Hursthouse, M. B. *J. Chem. Soc., Dalton Trans.* **1987**, 2723. (b) Cotton, F. A.; Labella, L.; Shang, M. *Inorg. Chem.* **1992**, *31*, 2385.
(9) (a) Cotton, F. A.; Falvello, L. R.; Han, S. *Inorg. Chem.* **1982**, *21*, 2889. (b) Kuz′menko, I. V.; Zhilyaev, A. N.; Fomina, T. A.; Porai-Koshits, M. A.; Baranovskii, I. B. *Russ. J. Inorg. Chem.* **1989**, *34*, 1457.
(10) (a) Bino, A.; Cotton, F. A. *Angew. Chem., Int. Ed. Engl.* **1979**, *18*, 462. (b) Cotton, F. A.; Han, S.; Conder, H. L.; Walton, R. A. *Inorg. Chim. Acta* **1983**, *72*, 191.
(11) Chang, H.-C.; Mochizuki, K.; Kitagawa, S. *Inorg. Chem.* **2005**, *44*, 3799−3809.
(12) Kondo, M.; Hamatani, M.; Kitagawa, S. *J. Am. Chem. Soc.* **1998**, *120*, 455.
(13) (a) Stephenson, T. A.; Wilkinson, G. *J. Inorg. Nucl. Chem.* **1966**, *28*, 2285. (b) Mitchell, R. W.; Spencer, A.; Wilkinson, G. *J. Chem. Soc., Dalton Trans.* **1973**, 846.

Table 1. Coordination Geometry around the Alkali-Metal Cations (A^+) Bound to $[Ru_2(R_4Cat)_4]^{2-/3-}$

	A^+	geometry[c]	environment	bond distances/Å
$[Na(THF)_5]$	Na^+	distorted Sp	$Na(O_{Cat})_2(H_2O)_3$	$Na-O_{Cat} = 2.500-2.515$, $Na-O_{H_2O} = 2.384-2.566$
$[\{Na(THF)(H_2O)_{1.5}\}_2$ $\{Ru_2(Cl_4Cat)_4(THF)\}]$[a,b]		distorted Sp distorted Sp	$Na(O_{Cat})_2(H_2O)_3$ $Na(O_{THF})_5$	$Na-O_{Cat} = 2.401-2.516$, $Na-O_{H_2O} = 2.408-2.463$ $Na-O_{THF} = 2.32-2.39$
$[Na\{Na(acetone)(H_2O)\}_2$ $\{Ru_2(Br_4Cat)_4\}]\cdot 2acetone$[a]	Na^+	distorted Sp distorted Sp distorted Sp	$Na(O_{Cat})_3(O_{acetone})(H_2O)$ $Na(O_{Cat})_3(O_{acetone})(H_2O)$ $Na(O_{Cat})_3(H_2O)_2$	$Na-O_{Cat} = 2.361-2.68$, $Na-O_{acetone} = 2.33$, $Na-O_{H_2O} = 2.32$ $Na-O_{Cat} = 2.322-2.66$, $Na-O_{acetone} = 2.29$, $Na-O_{H_2O} = 2.31$ $Na-O_{Cat} = 2.472-2.63$, $Na-O_{H_2O} = 2.35-2.37$
$[Na\{Na(DMF)\}_2$ $\{Ru_2(H_4Cat)_4\}]$[a]	Na^+	distorted Sp distorted Td distorted Sp	$Na(O_{Cat})_4(DMF)$ $Na(O_{Cat})_4$ $Na(O_{Cat})_4(DMF)$	$Na-O_{Cat} = 2.327-2.594$, $Na-O_{DMF} = 2.226$ $Na-O_{Cat} = 2.287-2.323$ $Na-O_{Cat} = 2.317-2.583$, $Na-O_{DMF} = 2.25$
$[\{Na(THF)(H_2O)\}_2$ $\{Ru_2(Cl_4Cat)_4(THF)_2\}]$[a,b]	Na^+	distorted Sp	$Na(O_{Cat})_2(THF)(H_2O)_2$	$Na-O_{Cat} = 2.384-2.464$, $Na-O_{THF} = 2.296$, $Na-O_{H_2O} = 2.418-2.442$
$[\{Na(THF)_2\}_2$ $\{Ru_2(Br_4Cat)_4(THF)_2\}]$[a]	Na^+	distorted Sp distorted Sp	$Na(O_{Cat})_3(THF)_2$ $Na(O_{Cat})_3(THF)_2$	$Na-O_{Cat} = 2.471-2.639$, $Na-O_{THF} = 2.36-2.37$ $Na-O_{Cat} = 2.478-2.509$, $Na-O_{THF} = 2.31-2.32$
1a	Li^+	distorted Oh	$Li(O_{Cat})_2(DME)_2$[d]	$Li-O_{Cat} = 2.067-2.377$, $Li-O_{DME} = 2.047-2.335$
1b[a]	Na^+	distorted Oh	$Na(O_{Cat})_2(DME)_2$[d]	$Na-O_{Cat} = 2.294-2.408$, $Na-O_{DME} = 2.322-2.493$
1c	K^+	distorted Tpr	$K(O_{Cat})_4(DME)$[d]	$K-O_{Cat} = 2.777-2.875$, $K-O_{DME} = 2.642-2.816$
1d	Rb^+	distorted Tpr	$Rb(O_{Cat})_4(DME)$[d]	$Rb-O_{Cat} = 2.897-2.968$, $Rb-O_{DME} = 2.797-2.935$
$\mathbf{2b_s}$[a]	Na^+	distorted Td	$Na(O_{Cat})_2(THF)_2$	$Na-O_{Cat} = 2.30-2.35$, $Na-O_{THF} = 2.25-2.47$

[a] Reference 11. [b] Reference 12. [c] Oh = octahedral, Sp = square pyramidal, Td = tetrahedral, and Tpr = trigonal prism. [d] Each DME chelates to the A^+ cation.

The resultant suspension was stirred for a day, giving a red-purple suspension, which was evaporated to dryness and then extracted with THF. Slow diffusion of hexane onto the solution gave a single crystal of $(n\text{-}Bu_4N)_2[Ru_2(3,6\text{-}DTBCat)_4]\cdot$hexane ($\mathbf{2e_s}$), which easily loses the cocrystallized solvent under vacuum. Yield: 220 mg (70%). Anal. Calcd for $C_{88}H_{152}N_2O_8Ru_2$ (**2e**): C, 67.39; H, 9.77; N, 1.79. Found: C, 67.29; H, 9.81; N, 1.73. UV−vis−NIR (λ_{max}/nm ($\epsilon/M^{-1}\cdot cm^{-1}$) in THF): 303 (23600), 396 (9300), 510 (11100), 650 (sh).

2.4. Physical Measurements. Absorption spectra were recorded on a Hitachi U-3500 spectrophotometer over the range 185−3200 nm at 296 K. Electrochemical measurements were carried out with a BAS model 650A electrochemical analyzer. A standard three-electrode system was used with a glassy carbon working electrode, platinum-wire counter electrode, and $Ag/Ag^+/CH_3CN$ electrode as reference (all of the potentials in the figures and table are given as volts vs ferrocene/ferrocenium (Fc/Fc^+)).

2.5. Crystallographic Data Collection and Refinement of Structures. All crystallographic measurements were performed on a Rigaku mercury diffractometer with a CCD two-dimensional detector with Mo Kα radiation employing a graphite monochromator. The sizes of the unit cells were calculated from the reflections collected on the setting angles of seven frames by changing ω by 0.5° for each frame. Two or three different χ settings were used, and ω was changed by 0.5° per frame. Intensity data were collected in 480−1080 frames with an ω scan width of 0.5°. Numerical absorption corrections were performed. All of the crystallographic data are summarized in Table 1. The structures were solved by the Patterson method[14] and expanded using Fourier techniques.[15] The final cycles of the full-matrix least-squares refinements were based on the observed reflections ($I > 3\sigma(I)$ for $\mathbf{2e_s}$ and $I > 4\sigma(I)$ for the others). All of the calculations were performed using the teXsan crystallographic software package from Molecular Structure Corp.[16] There is a highly disordered *t*-Bu group, C(26)−C(28), in **1a**.

3. Results and Discussion

3.1. Connection Modes of the Na^+ Cations to $[Ru_2(R_4Cat)]^{2-/3-}$ Units. Figure 1 schematizes the structures of the complexes $[Na_n\{Ru_2(R_4Cat)_4\}]$ ($n = 2$ or 3; $R_4 = Cl_4$, Br_4, H_4, 3,5-di-*t*-Bu, and 3,6-di-*t*-Bu), including the connection modes of the Na^+ cations to the O_{Cat} atoms. Table 1 lists the structural parameters around the cations. Two basic modes are found in connecting the Na^+ cations to the $[Ru_2(R_4Cat)]^{2-/3-}$ units. The first mode, called the "in-plane connection", was found in **1b** and $\mathbf{2b_s}$ (Figure 1a), where each Na^+ cation binds to two independent O_{Cat} atoms coming from two cofacial R_4Cat^{2-} anions. The Na^+ cations are further chelated by DME (**1b**) or coordinated by THF ($\mathbf{2b_s}$), exhibiting a distorted octahedral or tetrahedral coordination geometry. On the other hand, the second mode, called the "out-of-plane connection", was found in $[Na(THF)_5]$-$[\{Na(THF)(H_2O)_{1.5}\}_2\{Ru_2(Cl_4Cat)_4(THF)\}]$[11,12] (Figure 1b). The Na^+ cations connect two O_{Cat} atoms coming from two parallel Cl_4Cat^{2-} anions of each $[Ru(Cl_4Cat)_2]$ half. The connection modes in $[\{Na(THF)_2\}_2\{Ru_2(Br_4Cat)_4(THF)_2\}]$[11] (Figure 1c), $[Na\{Na(acetone)(H_2O)\}_2\{Ru_2(Br_4Cat)_4\}]\cdot$2acetone[11] (Figure 1e), and $[Na\{Na(DMF)\}_2\{Ru_2(H_4Cat)_4\}]$[11] (Figure 1f) are combinations of in-plane connection and out-of-plane connection. The H_2O molecules also take part in the bridging structures in $[\{Na(THF)(H_2O)\}_2\{Ru_2(Cl_4Cat)_4$-$(THF)_2\}]$[11,12] (Figure 1g), where the Na^+ cation having the in-plane connection mode and a H_2O molecule bridge two O_{Cat} atoms coming from the two cofacial Cl_4Cat^{2-} anions by hydrogen bonds ($O_{Cat}\cdots H-O = 2.82$ and 3.00 Å).

The connecting structures of the Na^+ cations to the $[Ru_2(R_4Cat)]^{2-/3-}$ units are among the fascinating features

(14) PATTY: Beurskens, P. T.; Admiraal, G.; Beurskens, G.; Bosman, W. P.; de Gelder, R.; Israel, R.; Smits, J. M. M. *The DIRDIF program system*; Technical Report of the Crystallography Laboratory; University of Nijmegen: Nijmegen, The Netherlands, 1994.

(15) DIRDIF94: Beurskens, P. T.; Admiraal, G.; Beurskens, G.; Bosman, W. P.; de Gelder, R.; Israel, R.; Smits, J. M. M. *The DIRDIF program system*; Technical Report of the Crystallography Laboratory; University of Nijmegen: Nijmegen, The Netherlands, 1994.

(16) *teXsan: Crystal Structure Analysis Package*; Molecular Structure Corp.: The Woodlands, TX, 1985, 1992.

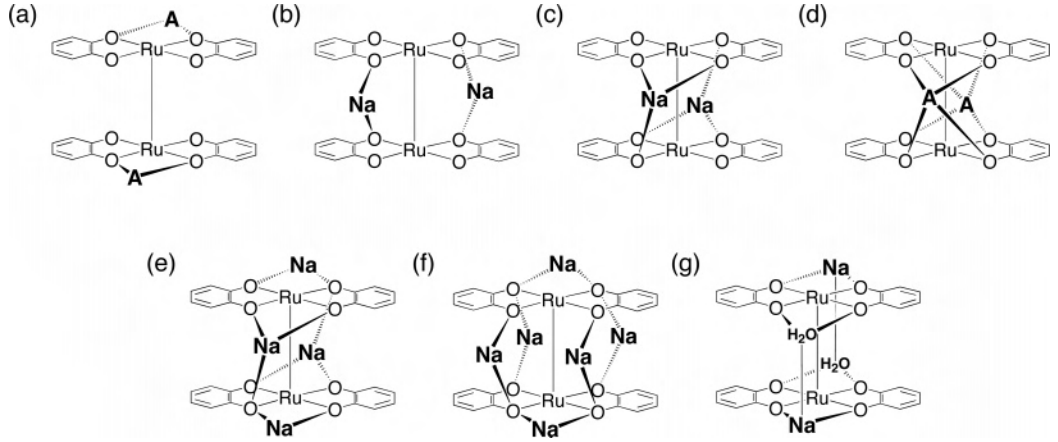

Figure 1. Schematic representation of connection modes of alkali-metal cations (A^+) bound to the $[Ru_2(R_4Cat)_4]^{2-/3-}$ units: (a) **1a**, **1b**, and **2b$_s$**, (b) $[Na(THF)_5][\{Na(THF)(H_2O)_{1.5}\}_2\{Ru_2(Cl_4Cat)_4(THF)\}]$,[11,12] (c) $[\{Na(THF)_2\}_2\{Ru_2(Br_4Cat)_4(THF)_2\}]$,[11] (d) **1c** and **1d**, (e) $[Na\{Na(acetone)(H_2O)\}_2\{Ru_2(Br_4Cat)_4\}]\cdot 2acetone$,[11] (f) $[Na\{Na(DMF)\}_2\{Ru_2(H_4Cat)_4\}]$,[11] (g) $[\{Na(THF)(H_2O)\}_2\{Ru_2(Cl_4Cat)_4(THF)_2\}]$.[11,12] The axial ligands, substituents of the catecholates, and solvent molecules that bind to the Na^+ cations are omitted for clarity.

Table 2. Crystallographic Data of $[\{A(DME)_n\}_2\{Ru_2(3,5\text{-DTBCat})_4\}]$ ($n = 2$ for $A^+ = Li^+$ (**1a**) and $n = 1$ for K^+ (**1c**) and Rb^+ (**1d**)) and $(n\text{-}Bu_4N)_2[Ru_2(3,6\text{-DTBCat})_4]\cdot$hexane (**2e$_s$**) with $[Ru_2]^{6+}$ Cores

	1a	**1c**	**1d**	**2e$_s$**
formula	$C_{72}H_{120}Li_2O_{16}Ru_2$	$C_{64}H_{100}K_2O_{12}Ru_2$	$C_{64}H_{100}O_{12}Rb_2Ru_2$	$C_{94}H_{166}N_2O_8Ru_2$
fw	1457.75	1341.82	1434.56	1654.49
cryst syst	monoclinic	trigonal	trigonal	monoclinic
space group	$P2_1/c$	$R\bar{3}$	$R\bar{3}$	$C2_1/c$
color of cryst	purple	purple	purple	purple
a, Å	11.1297(3)	30.572(3)	30.511(2)	25.481(7)
b, Å	16.192(1)			19.026(5)
c, Å	21.645(2)	19.309(3)	19.4609(1)	22.818(6)
β, deg	100.7951(4)			116.243(3)
V, Å^3	3831.6(4)	15629(1)	15689(1)	9921(4)
temp, K	223	223	223	223
Z	2	9	9	4
D_{calcd}, g·cm^{-3}	1.263	1.283	1.366	1.108
no. of reflns	6898[a]	4868[a]	5392[a]	6829[b]
no. of params	415	361	361	451
GOF	1.67	1.13	1.33	1.07
R_{int}	0.014	0.026	0.019	0.040
R, R_w[c]	0.033, 0.062	0.032, 0.042	0.049, 0.071	0.048, 0.067

[a] $I > 4.0\sigma(I)$. [b] $I > 3.0\sigma(I)$. [c] $R = \sum||F_o| - |F_c||/\sum|F_o|$, $R_w = [\sum w(|F_o| - |F_c|)^2/\sum w|F_o|^2]^{1/2}$.

of the present complexes, especially for the development of molecular assemblages based on cation···anion interactions. In fact, some of the complexes form infinite polymeric chains;[11] on the other hand, the cations prevent the formation of a ligand-unsupported M−M-bonded complex isolated from the cationic moieties. With these experimental results in mind, the following subjects must be experimentally demonstrated and reasonably understood. The structural effects of the cations on the $[Ru_2(R_4Cat)]^{2-/3-}$ units should be carefully examined, because the structures of the complexes with ligand-unsupported M−M bonds are expected to be very sensitive to the coordinative interaction and the electrostatic interaction of the cations. Electrochemical studies, for example, will answer the question of how the cations affect the properties of the complexes in solution.

3.2. Size Effects of the Cations on the Molecular Structures of a Family of $[A_2\{Ru_2(3,5\text{-DTBCat})_4\}]$ ($A^+ = Li^+$, Na^+, K^+, and Rb^+). To show the cation's effects on the structures, the size and nature of the cation were altered using a series of alkali-metal cations under conditions of constant substituents and oxidation state of the diruthenium complexes. Our synthetic attempts led to success in the systematic isolation and crystallographic structural characterization of a series of $[\{A(DME)_n\}_2\{Ru_2(3,5\text{-DTBCat})_4\}]$ ($n = 2$ for $A = Li^+$ (**1a**) and Na^+ (**1b**) and $n = 1$ for K^+ (**1c**) and Rb^+ (**1d**)) with four different countercations, which were introduced from LiOH, NaOH, KOH, and RbOH for the deprotonation of 3,5-DTBCatH_2 (Scheme 1).

The crystallographic data and the structural parameters of the complexes are listed in Tables 2 and 3. The molecular structures depicted in Figure 2 demonstrate that the crystal systems of **1a**−**1d** can be classified into two classes.[17] The complexes with Li^+ (**1a**) and Na^+ (**1b**) cations were crystallized in the isomorphous monoclinic space group, while those with K^+ (**1c**) and Rb^+ (**1d**) cations were in the isomorphous trigonal space group. In both isomorphous classes, the two complexes have quite similar unit cell parameters, although the complex with a smaller cation in each class has a slightly smaller cell volume. Interestingly, the isomeric forms of the $[Ru(3,5\text{-DTBCat})_2]$ unit in **1a**−**1d** do not vary with the cations; that is, all the complexes

(17) The crystallographic data of **1b** are as follows: monoclinic, $P2_1/c$, $Z = 2$, $a = 11.073(2)$ Å, $b = 16.211(2)$ Å, $c = 22.136(3)$ Å, $\beta = 100.146(3)°$, $V = 3911.5(9)$ Å^3, 223 K, $R = 0.040$, $R_w = 0.055$.

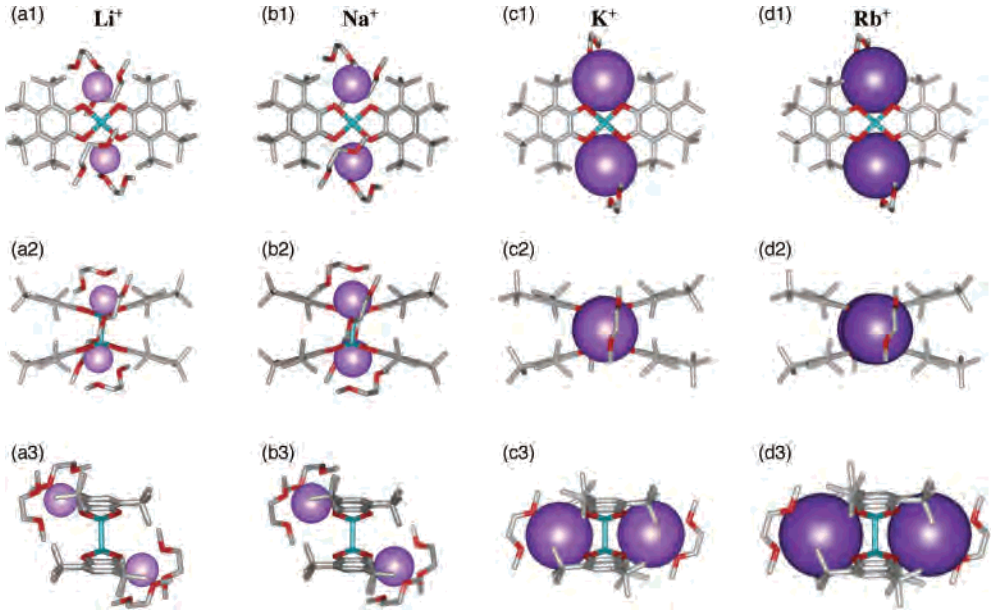

Figure 2. Whole molecular structures of $[A_2\{Ru_2(3,5\text{-DTBCat})_4\}]$ (A^+ = (a1−a3) Li^+ (**1a**), (b1−b3) Na^+ (**1b**), (c1−c3) K^+ (**1c**), and (d1−d3) Rb^+ (**1d**)) including the countercations: top view (top line), side view 1 (middle line), side view 2 (bottom line). Hydrogen atoms are omitted for clarity. Color code: Ru, deep green; C, gray; O, red; Li−Rb, violet.

Table 3. Structural Parameters of $[\{A(DME)_n\}_2\{Ru_2(3,5\text{-DTBCat})_4\}]$ (n = 2 for $A^+ = Li^+$ (**1a**) and Na^+ (**1b**) and n = 1 for K^+ (**1c**) and Rb^+ (**1d**)), $[\{Na(THF)_2\}_2\{Ru_2(3,6\text{-DTBCat})_4\}]$ (**2b$_s$**), and (n-$Bu_4N)_2[Ru_2(3,6\text{-DTBCat})_4]$·hexane (**2e$_s$**)

complex	A^+	Ru−Ru/ Å	Ru−O_{Cat}(av)/ Å	C−O_{Cat}(av)/ Å	deviation d/Å	Ru−Ru−O_{Cat}(av)/ deg	isomeric form	twist angle θ/deg	no. of axial ligands	assembled structure
1a	Li^+	2.1706(3)	1.968	1.366	0.4998(7)	104.23	*cis,cis-anti*	2.10	0	discrete
1b[a]	Na^+	2.1698(6)	1.969	1.363	0.486(1)	104.26	*cis,cis-anti*	1.58	0	discrete
1c	K^+	2.1820(5)	1.968	1.368	0.423(1)	102.41	*cis,cis-anti*	0.97	0	discrete
1d	Rb^+	2.1795(6)	1.970	1.366	0.426(1)	102.49	*cis,cis-anti*	1.10	0	discrete
2b$_s$[a]	Na^+	2.140(2)	1.97	1.37	0.509(5)	105.2		50.8	0	discrete
2e$_s$	n-Bu_4N^+	2.1449(7)	1.970	1.357	0.506(2)	104.87		48.9	0	discrete

[a] Reference 11.

have *cis*-configulated $[Ru(3,5\text{-DTBCat})_2]$ halves, and these are combined in an eclipsed form so that each half is related by 180° rotation around the Ru−Ru bond.[18] Each Ru atom has a five-coordinated square pyramidal geometry formed by an adjacent Ru atom and four O atoms from two coplanar dioxolene ligands, while there is a vacant site in the axial position. The binding modes of the cations can also be divided into two categories, depending on the size of the cations. As shown in Figure 2a,b, both cations in **1a** and **1b** have a distorted octahedral geometry and are effectively coordinated by two O_{Cat} atoms of two cofacial 3,5-$DTBCat^{2-}$ anions (Figure 1a) and four O_{DME} atoms from two DME molecules. The Li−O_{Cat} and Li−O_{DME} bond distances of **1a** are shorter than the corresponding Na−O_{Cat} and Na−O_{DME} distances of **1b**. When the size of the cation increases to that of K^+ or Rb^+, the coordination geometry of the cations changes to a distorted trigonal prism geometry. In these complexes, the cations locate between two $[Ru(3,5\text{-DTBCat})_2]$ planes by the out-of-plane connection as shown in Figure 2c,d and are coordinated by four O_{Cat} atoms of 3,5-$DTBCat^{2-}$ anions (Figure 1d) and further chelated by two O_{DME} atoms from a DME. The increase of the size of the cation induces the elongation of the A−O distances, as given in Table 1.

The Ru−O_{Cat} and C−O_{Cat} bond distances of **1a**, **1c**, and **1d** are in the range of 1.968−1.970 and 1.366−1.368 Å, respectively. These values are comparable to those of **1b**,[11] indicating the dianionic nature of the ligand moieties. Only small changes are observed in the Ru−Ru bond distances of the four complexes; those of **1a** and **1b** are slightly shorter than those of **1c** and **1d**, with the variation smaller than 0.015 Å. The deviation is much smaller than those of the Ru−Ru bond distances caused by the one-electron oxidations (ca. 0.03 Å) or the substituent effects (ca. 0.08 Å).[11] The most prominent difference is found in the d values and Ru−Ru−O_{Cat} angles, which reflect the degree of warp around the $[Ru_2]$ cores. The d values[19] for **1c** and **1d** are significantly

(18) Seven possible isomers are (a) a *cis,cis-syn* isomer, (b) a *cis,cis-anti* isomer, (c, d) two *cis,trans* isomers, (e) a *trans,trans-syn* isomer, and (f, g) two *trans,trans-anti* isomers, where the two isomers in two sets (c, d and f, g) are mirror images of each other (see the Supporting Information).

(19) See Chart 3 in ref 11.

Table 4. Redox Potentials (V vs Fc/Fc^+) of $[A_2\{Ru_2(3,5\text{-DTBCat})_4\}]$ ($A^+ = Li^+$ (**1a**), Na^+ (**1b**), K^+ (**1c**), and Rb^+ (**1d**)), $[Na_2\{Ru_2(3,6\text{-DTBCat})_4\}]$ (**2b**), and $(n\text{-}Bu_4N)_2[Ru_2(3,6\text{-DTBCat})_4]$ (**2e**)[a]

				redox potentials/V (ΔE_{pp}/V)		
complex	A^+	R_4	rest potential/V			$[Ru_2]^{6+}/[Ru_2]^{5+}$
1a	Li^+	3,5-DTB	−0.56		−0.33[c]	−1.16 (0.11)
1b[b]	Na^+	3,5-DTB	−0.59		−0.33[c]	−1.41 (0.21)
1c	K^+	3,5-DTB	−0.59		−0.33[c]	−1.52 (0.16)
1d	Rb^+	3,5-DTB	−0.68		−0.33[c]	−1.58 (0.10)
2b[b]	Na^+	3,6-DTB	−0.99	−0.35 (0.11)	−0.74 (0.09)	−1.46 (0.27)
2e	$n\text{-}Bu_4N^+$	3,6-DTB	−1.01	−0.34 (0.15)	−0.75 (0.11)	−2.38 (0.12)

[a] THF solution containing 2 mM complex and 0.2 M $n\text{-}Bu_4NPF_6$, 10 mV/s. [b] Reference 11. [c] E_{ap}.

reduced by ca. 0.06−0.08 Å, and the Ru−Ru−O_{Cat} angles simultaneously narrow by ca. 2° compared with those of **1a** and **1b**. These results can be interpreted by the differences in the connection mode of the cations. As a result, complexes **1c** and **1d** form slightly compacted structures with small *d* values compared with those of **1a** and **1b**. However, the effects of the cations seem weak in the solid state compared with those of the substituents or oxidation states.

3.3. Cation-Dependent Redox Properties. Turning now to the electrochemical properties of this series of compounds, interesting electrochemical features were observed, as described below. As shown in the preceding report,[11] complex **1b** undergoes a quasi-reversible one-electron redox couple at −1.41 V, which is attributable to the reduction of the $[Ru_2]$ core from $[Ru_2]^{6+}$ to $[Ru_2]^{5+}$. Systematic CV studies indicate that the overall features of cyclic voltammograms for **1a**−**1d** remain unchanged, demonstrating a quasi-reversible reduction process in the potential region of −1.16 to −1.58 V and irreversible oxidation from −0.30 to −0.33 V (Table 4). Interestingly, the redox potentials of the oxidation process show relatively small variations over the four complexes, while those for the reduction were significantly negatively shifted as the cation size increased (Figure 3a and Table 4). The half-wave potentials of the first reduction process were shifted negatively upon going from −1.16 V for **1a** to −1.41 and −1.52 V for **1b** and **1c**, respectively, and finally to −1.58 V for **1d**. The reduction potential of **1d** is greatly shifted by approximately 0.4 V compared with that for **1a**. The observed shifts of the redox potentials parallel the pattern in size/charge ratio of the cations ($r_{ionic}(Li^+) = 0.90$ Å, $r_{ionic}(Na^+) = 1.16$ Å, $r_{ionic}(K^+) = 1.52$ Å, $r_{ionic}(Rb^+) = 1.66$ Å) and may result merely from ion pairing, with the strongest interaction occurring with the ion of greatest ionic potential, Li^+. However, the results do not eliminate the possibility that the cations still bind to the $[Ru_2(3,5\text{-DTBCat})_4]^{2-}$ units in solution as well as in the solid state. This is because the binding affinity of the alkali-metal cations to the O atom are generally in the same order of $Li^+ > Na^+ > K^+ > Rb^+$, which is closely associated with the hydration energy.[20]

18-crown-6 was added to try to ensure that the species observed initially was complexed with the alkali-metal cations. Figure 3b shows the differential pulse voltammogram for **1c** with K^+ cations, which is known to exhibit the strongest binding affinity to 18-crown-6.[21] The first reduction process on the $[Ru_2]^{6+}$ core of **1c**, which appeared at −1.48 V, is quasi-reversible. Addition of 1 equiv of 18-crown-6 results in increases of the two peaks at −1.76 and −2.23 V; at the same time, the original peak tends to decrease in

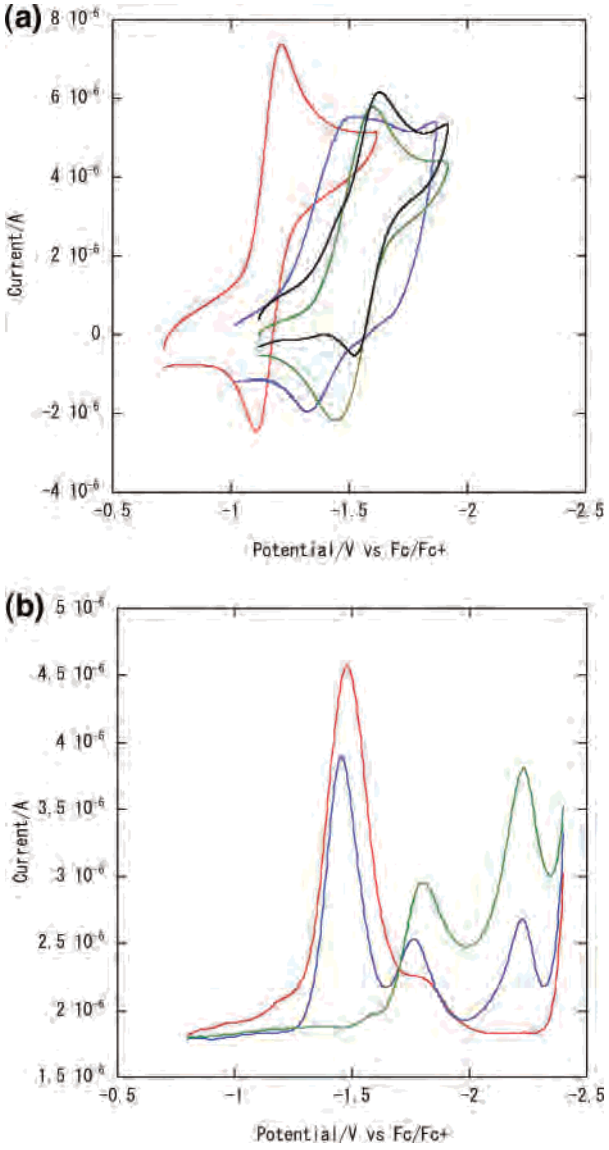

Figure 3. (a) Cyclic voltammograms of $[A_2\{Ru_2(3,5\text{-DTBCat})_4\}]$ ($A^+ = Li^+$ (**1a**, red line), Na^+ (**1b**, blue line), K^+ (**1c**, green line), and Rb^+ (**1d**, black line)) without 18-crown-6. Conditions: 2 mM THF solution containing 0.2 M $n\text{-}Bu_4NPF_6$, 10 mV/s, room temperature, N_2. (b) Differential pulse voltammogram of $[K_2\{Ru_2(3,5\text{-DTBCat})_4\}]$ (**1c**) without 18-crown-6 (red line) and with 1 equiv (blue line) and 2 equiv (green line) of 18-crown-6 in THF. Conditions: 1 mM THF solution containing 0.1 M $n\text{-}Bu_4NPF_6$, room temperature, N_2, *E* increment 0.004 V, pulse width 0.05 s, sample width 0.0167 s, pulse period 0.2 s.

(20) Metelski, P. D.; Swaddle, T. W. *Inorg. Chem.* **1999**, *38*, 301.

intensity. Further addition of 1 equiv of 18-crown-6 causes increases of the intensity of the two peaks, with a decease of the original peak. The redox potentials obtained after the addition of 2 equiv of 18-crown-6 are shifted in potential by 0.32 and 0.75 V, respectively, relative to that of **1c**. The appearance of two new peaks could be reasonably understood by the presence of diruthenium complexes bound with one K^+ cation and without a K^+ cation, which are generated by removing complexed K^+ cations by 18-crown-6. Thus, these results demonstrate the electrostatic effect of K^+ bound in close proximity to the $[Ru_2(3,5\text{-}DTBCat)_4]^{2-}$ units.

Significant cation-modulated electrochemical effects are principally due to the cation-bound molecular structures, where the ionophore moiety is very close to the redox center of the $[Ru_2(3,5\text{-}DTBCat)_4]^{2-}$ units. The negative shift of the reduction potentials could be reasonably understood in terms of the efficacy of the electrostatic stabilization effect of the cation against the electrochemically generated $[Ru_2(3,5\text{-}DTBCat)_4]^{3-}$ species. A greater stabilization effect is established in **1a** with the Li^+ cation by its strong coordination and small r_{ionic} (resulting in a high positive charge density). When the size of the cation increases, both effects weaken, thereby destabilizing the $[Ru_2(3,5\text{-}DTBCat)_4]^{3-}$ species, and the reduction potential shifts negatively.

3.4. Inherent Stability of the Ligand-Unsupported Ru−Ru Bonds. The previous section demonstrated that although the countercations do not induce a drastic perturbation in the intramolecular structural parameters of the complexes, they play important roles in their electrochemical properties. These results clearly demonstrate that the anionic nature of the $[Ru_2(R_4Cat)_4]^{2-/3-}$ moieties provides a means to tune the properties of the complexes through both the electrostatic interactions and the binding interactions of the cations. It is, however, important that any structural and electronic effects derived from the binding structures of the cations shown in Figures 1 and 2 could not be excluded at this stage. In other words, the ambiguity in the inherent ability of the R_4Cat^{2-} ligands to stabilize the ligand-unsupported Ru−Ru-bonded structures still remains.

The treatment of **2b** with *n*-Bu_4NPF_6 smoothly results in a cation exchange reaction, leading to the formation of (*n*-$Bu_4N)_2[Ru_2(3,6\text{-}DTBCat)_4]$·hexane (**2e$_s$**) at room temperature. The molecular structure depicted in Figure 4 clearly shows the formation of a cation-free structure, in keeping with a direct Ru−Ru bond, which is retained even after the cation exchange reaction. Any bridging mode could not be found within the $[Ru_2(3,6\text{-}DTBCat)_4]^{2-}$ unit, and the *n*-Bu_4N^+ cations exist far from the anionic complex. Two cofacial $[Ru(3,6\text{-}DTBCat)_2]$ halves are linked by the Ru−Ru bond, and no axial ligand was found on the Ru atoms, forming a pseudo square pyramidal coordination geometry similar to that of **2b$_s$**.[11]

Comparison of the structural parameters of **2b$_s$** and **2e$_s$** could be apparently useful to determine the cation effects in the solid state. Surprisingly, the structural parameters of both

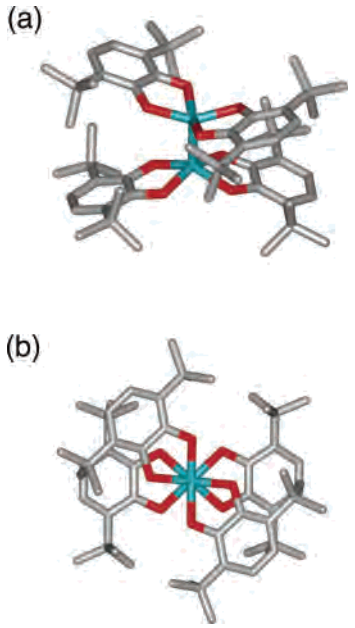

Figure 4. (a) Side and (b) top views of dianionic units in (*n*-$Bu_4N)_2[Ru_2(3,6\text{-}DTBCat)_4]$·hexane (**2e$_s$**). Hydrogen atoms, cations, and cocrystallized solvent molecules are omitted for clarity. Color code: Ru, green; C, gray; O, red.

complexes are almost unchanged, as listed in Table 3. The Ru−Ru bond distance of **2e$_s$** is 2.1449(7) Å, which is quite similar to the value of 2.140(2) Å for cation-bound **2b$_s$**. In addition, the *d* and θ values[19] are found to be 0.506(2) Å and 48.9° for **2e$_s$**, respectively, nearly equal to 0.509(5) Å and 50.8° for **2b$_s$**. All these data strongly support the conclusion that structural effects coming from the connection of the cation could almost be negligible. Therefore, the inherent ability of the R_4Cat^{2-} ligands stably to form the direct Ru−Ru bonds is now proved.

In contrast to the static molecular structure, the situation seems to be different in solution. As shown in Figure 5, the cyclic voltammogram of **2e** measured in THF solution consists of a quasi-reversible redox couple at −2.38 V and two quasi-reversible redox couples at −0.75 and −0.34 V as the first and second oxidation processes, respectively. The reduction potential of the complex shifts negatively compared with that of **2b** by ca. 0.9 V, reflecting the decreasing stability of the diruthenium complex with the $[Ru_2]^{5+}$ core. The negative shift of the reduction potential is just the same as the experimental result for the addition of 18-crown-6 to the solution containing **1c** (see section 3.3). Therefore, these results can be commonly understood in terms of the electrostatic and the binding effects of the cations, which directly affect the stability of the reductive products.

Figure 6 shows the UV−vis−NIR spectra of **2b** and **2e** measured in THF and DMF. The spectrum of **2b** in THF consists of a strong charge-transfer band at 514 nm with a shoulder at 700 nm. On the other hand, a new band appears around 400 nm in the spectrum of **2e** in THF. Interestingly, a similar absorption band around 400 nm could be observed also in the spectrum of **2b** measured in DMF solution. The observed spectral differences could be most plausibly attributed to the solvent polarity. In solvents with low polarity

(21) Pederson, C. J.; Frensdorff, H. K. *Angew. Chem., Int. Ed. Engl.* **1972**, *84*, 16.

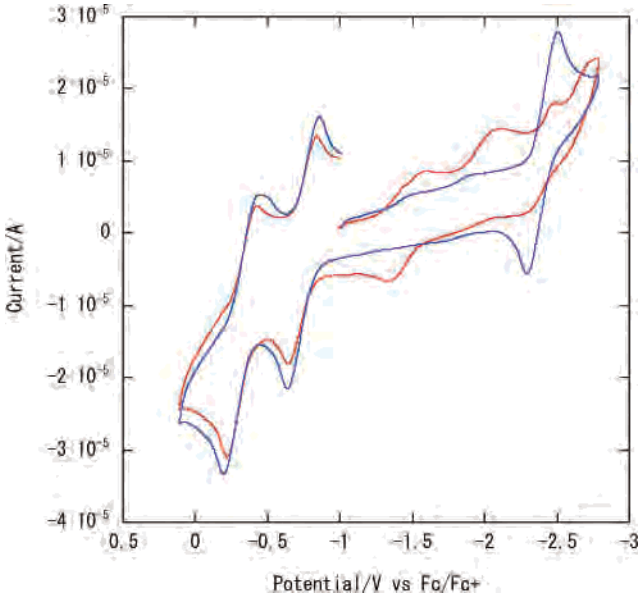

Figure 5. Cyclic voltammograms of $[Na_2\{Ru_2(3,6\text{-DTBCat})_4\}]$ (**2b**, red line) and $(n\text{-Bu}_4N)_2[Ru_2(3,6\text{-DTBCat})_4]$ (**2e**, blue line) in THF. Conditions: 2 mM THF solution containing 0.2 M $n\text{-Bu}_4NPF_6$, 100 mV/s, room temperature, N_2.

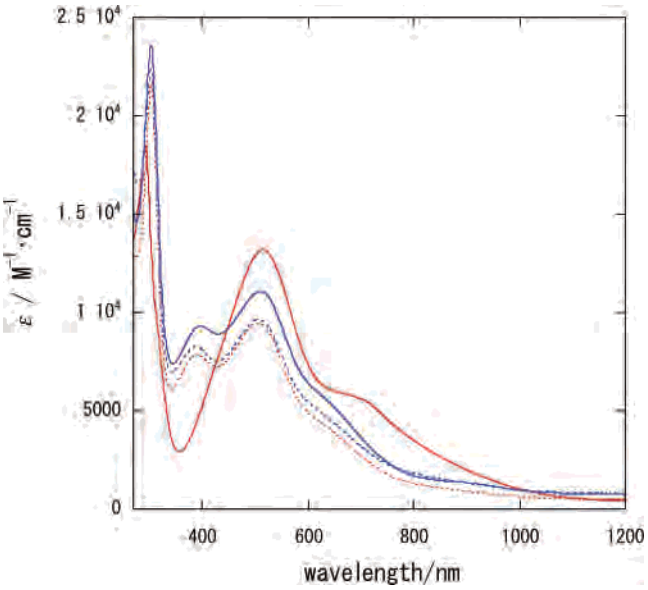

Figure 6. UV−vis−NIR spectra of $[Na_2\{Ru_2(3,6\text{-DTBCat})_4\}]$ (**2b**, red lines) and $(n\text{-Bu}_4N)_2[Ru_2(3,6\text{-DTBCat})_4]$ (**2e**, blue lines) in THF (solid lines) and DMF (dashed lines) at room temperature.

(THF), the alkali-metal cations still bind to the $[Ru_2(3,6\text{-DTBCat})_4]^{2-}$ unit with $Na-O_{Cat}$ bonds or closely pair ionically with the core by static interactions, while both interactions would be weakened in solvents with relatively high polarity (DMF). A similar trend can be found in the spectra of **1b** measured in THF and DMF (Figure S3 in the Supporting Information). As a result, one can then differentiate a cation-bound dimeric structure from a cation-free structure on the basis of UV−vis spectral patterns, together with their electrochemical properties. (See Table 5 for **1a**−**1d**, **2b**, and **2e**.)

Table 5. UV−vis−NIR Absorption Spectral Data of $[A_2\{Ru_2(3,5\text{-DTBCat})_4\}]$ ($A^+ = Li^+$ (**1a**), Na^+ (**1b**), K^+ (**1c**), and Rb^+ (**1d**)), $[Na_2\{Ru_2(3,6\text{-DTBCat})_4\}]$ (**2b**), and $(n\text{-Bu}_4N)_2[Ru_2(3,6\text{-DTBCat})_4]$ (**2e**)

complex	R_4	A^+	peak maxima/nm (ϵ/M^{-1} cm^{-1})
1a[b]	3,5-DTB	Li^+	294 (27800), 501 (16500), 700 (sh)
1b[a,b]	3,5-DTB	Na^+	299 (29000), 420 (sh), 518 (15200), 700 (sh)
1b[c]	3,5-DTB	Na^+	303 (24200), 375 (9000), 527 (11800)
1c[b]	3,5-DTB	K^+	298 (24600), 494 (16800), 720 (sh)
1d[b]	3,5-DTB	Rb^+	299 (26400), 486 (17700), 570 (sh), 720 (sh)
2b[a,b]	3,6-DTB	Na^+	293 (17800), 514 (12700), 700 (sh)
2b[c]	3,6-DTB	Na^+	304 (21700), 390 (7900), 507 (9500), 700 (sh)
2e[b]	3,6-DTB	$n\text{-Bu}_4N^+$	303 (23600), 396 (9300), 510 (11100), 650 (sh)
2e[c]	3,6-DTB	$n\text{-Bu}_4N^+$	303 (22400), 389 (8300), 507 (9600), 700 (sh)

[a] Reference 11. [b] Each spectrum was measured in THF. [c] Each spectrum was measured in DMF.

4. Conclusion

In this study, we have examined the effects of the countercations affecting the structural, electrochemical, and spectrochemical properties of the diruthenium complexes with ligand-unsupported Ru−Ru bonds containing catecholate derivatives. The results of the study can be summarized as follows. (1) The anionic nature of the diruthenium complexes provides considerable cation···anion interactions through both electrostatic and binding interactions. In addition to the binding structure in the solid state, these interactions play an important role in the electrochemical properties in solution. Moreover, recent preliminary results indicate that an isomeric form of $[Ru_2(3,5\text{-DTBCat})_4]^{2-}$, which can be from seven different isomeric forms (see the Supporting Information), is able to change to another by heating in solution. (2) Formation of the complex with a cation-free structure leads us to conclude that the high negative charge of R_4Cat^{2-} can stably form direct Ru−Ru bonds without any bridging and supporting species. The results of this study illustrate successive strategies of controlling the characteristic structures and properties of ligand-unsupported M−M systems by countercations and open a new route to design multifunctional M−M-bonded complexes.

Acknowledgment. We acknowledge financial support by a Grant-in-Aid for Scientific Research from The Ministry of Education, Culture, Sports, Science, and Technology of Japan.

Supporting Information Available: Figures of isomers for $[Ru_2(3,5\text{-DTBCat})_4]^{2-}$ and absorption spectra of **1a**−**1d** (PDF) and X-ray crystallographic data for **1a**, **1c**, **1d**, and $\mathbf{2e}_s$ in CIF format. This material is available free of charge via the Internet at http://pubs.acs.org.

IC048250U